Journal of Biomedical Optics

SPIEDigitalLibrary.org/jbo

Single photon counting fluorescence lifetime detection of pericellular oxygen concentrations

Neveen A. Hosny
David A. Lee
Martin M. Knight

SPIE

Single photon counting fluorescence lifetime detection of pericellular oxygen concentrations

Neveen A. Hosny,[a,b] David A. Lee,[a] and Martin M. Knight[a]
[a]University of London, School of Engineering and Materials Science, Queen Mary, London, United Kingdom, E1 4NS
[b]University of London, School of Biological and Chemical Science, Queen Mary, London, United Kingdom, E1 4NS

Abstract. Fluorescence lifetime imaging microscopy offers a non-invasive method for quantifying local oxygen concentrations. However, existing methods are either invasive, require custom-made systems, or show limited spatial resolution. Therefore, these methods are unsuitable for investigation of pericellular oxygen concentrations. This study describes an adaptation of commercially available equipment which has been optimized for quantitative extracellular oxygen detection with high lifetime accuracy and spatial resolution while avoiding systematic photon pile-up. The oxygen sensitive fluorescent dye, tris(2,2′-bipyridyl)ruthenium(II) chloride hexahydrate $[Ru(bipy)_3]^{2+}$, was excited using a two-photon excitation laser. Lifetime was measured using a Becker & Hickl time-correlated single photon counting, which will be referred to as a TCSPC card. $[Ru(bipy)_3]^{2+}$ characterization studies quantified the influences of temperature, pH, cellular culture media and oxygen on the fluorescence lifetime measurements. This provided a precisely calibrated and accurate system for quantification of pericellular oxygen concentration based on measured lifetimes. Using this technique, quantification of oxygen concentrations around isolated viable chondrocytes, seeded in three-dimensional agarose gel, revealed a subpopulation of cells that exhibited significant spatial oxygen gradients such that oxygen concentration reduced with increasing proximity to the cell. This technique provides a powerful tool for quantifying spatial oxygen gradients within three-dimensional cellular models.
 [DOI: 10.1117/1.JBO.17.1.016007]

Keywords: chondrocytes; oxygen gradients; ruthenium; extracellular; fluorescence lifetime; multi-photon microscopy; fluorescence lifetime imaging microscopy; time-correlated single photon counting.

Paper 11458P received Aug. 24, 2011; revised manuscript received Oct. 21, 2011; accepted for publication Nov. 14, 2011; published online Feb. 6, 2012.

1 Introduction

Eukaryotic cells depend on dioxygen, O_2 for production of cellular energy in the form of ATP via aerobic respiration. Variation of extracellular oxygen concentrations influences cellular metabolism and is key to tissue development and function. Methods that have been used to examine oxygen gradients in tissue or three-dimensional constructs include computational modeling,[1] photo-acoustic microscopy,[2] electron paramagnetic resonance combined with magnetic resonance imaging,[3,4] invasive probes, and non-invasive luminescence.[5,6] Modeling approaches rely heavily on experimental data using the Michaelis-Menten equation to describe the maximum oxygen consumption rate of cells [7] combined with Fick's 2nd law governing diffusion to estimate macro-gradients in tissues or constructs.[1] However, estimation of macro-environmental conditions may not be representative of the pericellular microenvironment that is influenced by microgradients directly around individual cells. Obtaining information in close proximity to the cell periphery requires high spatial resolution, <1 μm, and the flexibility of detection in different solutions unattainable through photo-acoustic microscopy, electron paramagnetic resonance or magnetic resonance imaging. The only remaining methods are invasive probes and non-invasive luminescence.

Invasive probes, such as the Clark's electrodes [5,8] or optrodes,[6,9,10] are able to derive oxygen measurements from within a three-dimensional cell system. The invasive nature of the probe causes damage to the surrounding site and, in the case of the electrode, directly consumes oxygen at a rate of 0.4 5 pmol/h thereby influencing the measured oxygen environment.[11] For both probes, the spatial resolution is limited by the size and surface area of the probe head with measurements restricted to a single point.[12] These probes also lack the ability of registering the measurement location. Alternatively, luminescence utilizes fluorescence or phosphorescence to measure the intensity or lifetime of a fluorophore.[12,13] Luminescence applied non-invasively, and used with lifetime rather than intensity, results in measurements that are independent of probe concentration, photobleaching and excitation drifts.[14]

Lifetime measurements are conducted using time resolved techniques based on the time or frequency domain, although commercially available equipment tends to focus on the former.[15–17] The two methods generally used for acquisition of lifetime data are time-gate or time-correlated single photon counting (TCSPC) methods. TCSPC is generally applied to confocal laser scanning microscopes,[18] whereas, time-gate is predominately used on widefield set-ups.[19] The advantage of TCSPC over time-gate relates to the low-photon counting noise during decay acquisition and the superior time-resolution for photon count registration.[20] In these studies, a two-photon excitation confocal system was used to aid excitation within 3D tissue

Address all correspondence to: Neveen A. Hosny, University of London, School of Engineering and Materials Science, Queen Mary, London, United Kingdom, E1 4NS; E-mail: n.hosny@imperial.ac.uk

0091-3286/2012/$25.00 © 2012 SPIE

constructs. This takes advantage of tissues natural transparency at IR wavelengths and provides optical sectioning that minimizes tissue exposure and fluorophore photobleaching. TCSPCs time-to-analogue converter has a time range limit of 2 μs restricting the maximum lifetime of any dye.

All fluorophores experience some form of quenching effects from oxygen,[21] but certain dyes exhibit a greater sensitivity to oxygen. In particular, polycyclic aromatic hydrocarbons, metalloporphyrin and transition metal polypyridyls such as, pyrene, platinum, palladium, and ruthenium have been used extensively. Pyrenebyutic acid has previously been used for intracellular measurements of oxygen concentration in rat liver cells.[22] However, there are number of factors that make these derivative unsuitable as an oxygen sensitive dye. For example, emission overlap with autofluorescence, poor chemical- and photostability,[23] limited sensitivity in the physiological range[24] and quenching caused by reactive oxygen species.[25] Platinum and palladium based probes have phosphorescent decays allowing encapsulation which protects it from the applied environment. However, only single point measurements are collated due to the restriction in acquisition speed derived from the long lifetime decay.[26,27] Ruthenium(II) complexes have been used for the detection and quantification of oxygen *in-vitro*[28] and *in-vivo*[27,29] and have lifetimes in the order of 600 ns making them suitable for TCSPC detection. The other advantages of ruthenium(II) complexes in homogeneous solution are the linear response to oxygen concentration,[30] large Stokes shift which provides high photo-stability,[31] and a lifetime longer than endogenous fluorophores and mono-exponential decay. Tris(2,2'-bipyridyl)ruthenium(II) chloride hexahydrate, $[Ru(bipy)_3]^{2+}$, is the least likely to bind to protein and DNA,[32] is hydrophilic, and inexpensive.

Dobrucki[33] investigated the impact of laser excitation on $[Ru(bipy)_3]^{2+}$ and $[Ru(phen)_3]^{2+}$ incubated with macrophage cells. His research suggested that the creation of reactive oxygen species from the illumination of $[Ru(bipy)_3]^{2+}$ and $[Ru(phen)_3]^{2+}$ lead to cellular membrane permeability, collapse, and eventually cell death. The concentration level at which phototoxicity occurs is disputed among researchers and can be between 0.2 mM to 1.34 mM.[28,33] This variation in concentration may be due to differences in the excitation source which may be pulsed or continuous, method of excitation which may be widefield or confocal, number of illuminations and illumination time period. Reactive oxygen species can also induce damage to the dye causing increased photobleaching. This has been shown in systems where $[Ru(bipy)_3]^{2+}$ was embedded in silica.[34] In this case, the restriction to diffusion prevents radical oxygen dissipating away from the dye and has a higher likelihood of reacting with the immediate environment causing photobleaching. The dependence of phototoxicity on excitation variables highlights the importance of conducting independent assessments on each system.

The present study investigates the suitability of $[Ru(bipy)_3]^{+2}$ using commercially available equipment for accurately measuring spatial oxygen gradients at <400 nm spatial resolution. Concentration dependence was previously tested using a range of concentrations between 0.104 to 3.34 mM and showed a linear relationship with intensity, but no effect on lifetime.[35] This techniques utilizes a fluorescence lifetime imaging microscopy (FLIM) TCSPC system with multi-photon laser and pulse-picker, which will reduce the 80 MHz laser repetition rate to accommodate the long lifetime of $[Ru(bipy)_3]^{+2}$ which is (<600 ns at 21 °C). The oxygen consumption of primary chondrocytes, as used in this study, is of particular interest given their specialist metabolism associated with the avascular nature of articular cartilage. Furthermore, there is increasing interest in the use of tissue engineered techniques for articular cartilage repair that require the culture of chondrocytes in monolayer or 3D systems. The agarose model has been well characterized in numerous previous studies and has demonstrated the ability to maintain chondrocytic phenotype with the production of cartilaginous extracellular matrix. However, the oxygen consumption and spatial gradients are unclear, hence the requirement for a non-invasive technique that is capable of providing high spatial resolution. Using this technique, spatial oxygen gradients were quantified for the first time around individual viable cartilage cells or chondrocytes which have been seeded in three-dimensional agarose constructs.

2 Instrumentation

The excitation was provided from a tuneable 720 to 990 nm multi-photon 80 MHz Mai Tai laser which was manufactured by Sapphire, Newport Spectra-Physics in the United Kingdom, and was subsequently delivered to a pulse-picker which was a Model 3980 which was manufactured by Newport Spectra-Physics in the United Kingdom. The laser excitation rate was controlled via a pulse selector Model 3986 which was manufactured by Newport Spectra-Physics in the United Kingdom, that provided a selection of repetition rates between 8 MHz down to single shot. After exiting the pulse-picker, a beam splitter created a reference beam to log excitation pulses using a photon counter PHD-400N manufactured by Becker & Hickl GmbH in Germany. Prior to the laser beam entering the Leica SP2 confocal microscope DM IRE2 which was manufactured by Leica-Microsystems Ltd. in the United Kingdom, the laser power was controlled via an electro-optical modulator LIV20 to 60 produced in Linos, Germany, as represented by the schematic in Fig. 1. Photon emission was collected with a photo-multiplier tube detector PMH-100, manufactured by Becker & Hickl GmbH in Germany is based on Hamamatsu H5773P module,

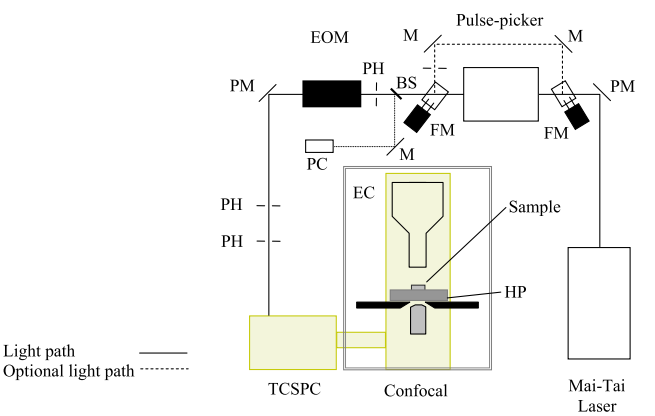

Fig. 1 Schematic layout of the MP-FLIM system. Abbreviations: PM—periscope mirror, FM—Flip mirror, M—Mirror, BS—Beam splitter, PC—Photon counter, PH—Pinhole, EOM—electro-optical modulator, TCSPC—Time correlate single photon counting module, EC—Environmental chamber, HP—Heating plate.

attached to the side port of the confocal microscope and was coupled to the Time-Correlated Single Photon Counting module SP830, enabling lifetime measurements.

The method of photon collection using TCSPC is fully described in the Becker & Hickl textbook.[36] To summarize, photon detection is discriminated from noise using a constant fractional discriminator. The signal is converted from analog to digital counts that are assigned by arrival time to the correct time channel. This is represented by a histogram depicting the decaying fluorophores after excitation and reflects the fluorophore's environment. Collection rates were maintained at $\leq 1\%$ of the repetition rate to avoid systematic pile inducing artificial lifetime components in the decay during collection.[37]

During experimentations, a repetition rate of 500 kHz at 780 nm was delivered through ×63 (NA 1.4) oil immersion objective lens 506192, HCX PL APO, Leica-Microsystems Ltd., GmbH, and produced a maximum power of 164 μW at the sample. The sample was measured using a Model 1830 power meter and a 818 IR/CW detector which were both manufactured by Newport Physics in the United Kingdom. All imaging was performed with the ×63 objective and using TCSPC settings of ADC 1024, unless otherwise stated.

3 Materials & Methodology

3.1 *Chemical Reagents and Preparation of Cell-Seeded Constructs*

Cell culture media consisted of standard Dulbecco's Modified Eagle Medium supplemented with 3.8 g/l HEPES, 80.6 U/ml penicillin and 80.6 mg/l streptomycin, 0.12 g/l L-ascorbic acid (A0278), 1% L-glutamine and 16% (v/v) fetal bovine serum. Calcein AM and Ethdium homodimer-2 were used as live and dead cell stains, respectively, at concentration of 5 μl/ml. Constructs were created with agarose powder which was dissolved in Hanks balance salt solution, autoclaved for 45 min and incubated in a 60 °C oven for 1 h, to create a sterilized solution which was cooled to 37 °C prior to mixing with cells. The oxygen sensitive dye used was Tris(2,2'-bipyridyl)ruthenium(II) chloride hexahydrate $[Ru(bipy)_3]^{2+}$. A filtered stock solution of $[Ru(bipy)_3]^{2+}$ was prepared with de-ionized water at a concentration of 13.34 mM.

3.1.1 *Cell preparation*

Primary chondrocyte-agarose constructs were prepared following the well established model and protocols described in numerous previous studies.[38–40] Briefly, cartilage was dissected under sterile conditions from the proximal surface of adult bovine metacarpal-phangel joints. Tissue from each joint, $n = 3$, was sequentially digested at 37 °C, with pronase and collagenase for one and 14 h, respectively. The digested cell suspension was passed through a 70 μm nylon cell strainer, washed three times with DMEM + 16%FBS, pooled together and the isolated cells were resuspended in 30 ml fresh DMEM + 16%FBS. Cells were seeded in 3% (w/v) agarose at 4×10^6 cell/ml and 20×10^6 cell/ml for pericellular measurements and viability tests, respectively. The cell-agarose mixture was gelled at 4 °C for 20 mins in specially designed air-tight chambers, as shown in Fig. 2. For pericellular measurements, quarter sections were removed using a sterile scalpel blade to provide even and rapid access for nutrients, oxygen and fluorophore. Each chamber was filled with 1 ml of media, loosely capped and left overnight in a 5% CO_2 incubator at 37 °C. Media was replaced 1.5 h prior to the experiment with a working concentration of $[Ru(bpy)_3]^{2+}$ media and incubation was continued.

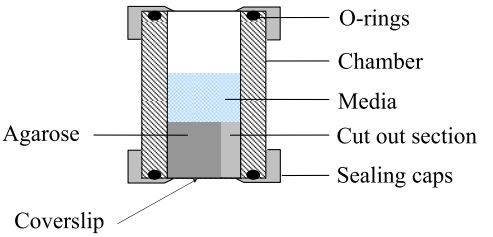

Fig. 2 Schematic of the sample chamber containing agarose construct filled with media.

3.2 *Ruthenium Characterization*

3.2.1 *Effects of temperature variation on lifetime*

Pre-calibration of the stage mounted heating plate, located within the environmental chamber, was completed prior to experiments using a digital handheld T-type thermocouple temperature sensor at an accuracy of ±0.2 °C. A single chamber, normally used for air-tight measurements, was filled with a 0.412 mM solution of $[Ru(bipy)_3]^{2+}$ in de-ionized water. Direct temperature measurements of the solution were performed using the digital thermocouple positioned at the center of the coverslip inside the chamber. The thermocouple was sealed into position using 12 sections of parafilm to restrict sample solution evaporation. The stage mounted heating plate was adjusted to provide a fine temperature control of 32 to 39 °C with temperature increments of 1 to 2 °C. Temperatures were set and the system was left to stabilize for 40 min between increments and lifetime decays were collected for 400 s. The temperatures were noted at the start and completion of each lifetime measurements to account for possible drift during the experiment.

3.2.2 *Effect of pH concentration on lifetime*

Pre-prepared solutions of phosphate buffer, K_2HPO_4, at a concentration of 50mM and pH values of 4 and 9 were combined to create six 1 ml aliquots with pH ranging between pH 5 to 7.5 with pH 0.5 increments. The final pH concentrations were confirmed using a 3 mm specialist pH meter with an accuracy of ±0.002 pH. The stock solution of $[Ru(bipy)_3]^{2+}$ was combined with the desired pH range to produce a final working concentrations of 0.412 mM. Each concentration was transferred into the wells of a glass bottomed 12 multi-well dish and mounted on the microscope stage. Measurements were performed at room temperature, 25 °C, and the decay was collected for 150 s. Five replicate lifetimes were measured for each pH concentration.

3.2.3 *Effect of fetal bovine serum (FBS) concentrations on lifetime*

The stock solution of $[Ru(bipy)_3]^{2+}$ was diluted in de-ionized water and FBS to produce nine FBS concentrations between 0 to

40% and a final $[Ru(bipy)_3]^{2+}$ concentration of 0.412 mM. The stock solutions were mixed by inversion before pipetting. For intensity measurements, five 200 μl aliquots of each concentration were transferred to a 96 well plate and excited using a fluorescence fluorimeter. The excitation and emission filters were set to 485 nm and 610 ± 10 nm, respectively. The fluorimeter used a xenon flash lamp with 50 excitation cycles and a gain adjustment of 48.

Time-resolved and emission spectrum measurements were carried out on the TP confocal FLIM system. The multiple repeats used for the intensity measurements were recombined and transferred to single wells of a glass-bottomed 12 well dish and mounted on the microscope stage. Five decays were collected for 100 s at 500 kHz and converted to ASCII files before imported into Origin. Single exponential decays were fitted between 200 and 1500 ns for each file. The emission spectrum of each dilution was measured between 500 to 750 nm in 5 nm increments. Images at each wavelength were captured with 2 line and frame scans and analyzed using the Leica stack profiling tool to produce the emission spectrum which was then exported to Origin. All measurements were performed at room temperature.

3.2.4 *Oxygen lifetime calibration*

Working concentrations of $[Ru(bipy)_3]^{2+}$ in de-ionized water and in media were prepared and added as 500 μl aliquots to six specially designed air-tight sample chambers. Chambers were equilibrated prior to each measurement at 37 °C for 24 h using a gas concentration of 0.1%, 1%, 5%, 10%, 15%, 19% O_2, 5% CO_2 and N_2 balance. This was achieved using a self-contained incubation system consisting of one main gloved chamber and two hydrated incubators with independent gas and temperature closed-loop computer control with an accuracy and precision of 0.1%. The XVivo system was calibrated using research grade N_2 gas and air balance cylinders to replicate zero and atmospheric oxygen using an inbuilt calibration facility.

Samples were sequentially mounted on to the microscope where the environmental chamber was maintained at a controlled ambient temperature of 35 °C and the stage mounted heating plate provided finer temperature control calibrated at 37 ± 0.2 °C. Decays were acquired post equilibration on the FLIM system at a repetition rate of 500 kHz collected at a count rate of less than 1% and a repetition rate for 800 s with 10 repeats. Decays where exported to Origin and mono-exponential decays fitted to calculate the lifetime for each sample, τ. Using the Stern-Volmer equation (1), lifetimes were correlated to oxygen concentrations to establish a representative relationship

$$\frac{\tau_0}{\tau} = 1 + K_{sv}[O_2], \tag{1}$$

where $[O_2]$ is the oxygen concentration, τ_0 is the lifetime with no quencher, τ is the measured lifetime, K_{SV} is the Stern-Volmer constant; $K_{SV} = \tau_0 \cdot k_2$ where k_2 is is the sum of all the bimolecular rate constants for all bimolecular excited state deactivations describing the interaction between the dye and quencher within its environment.[41] Relating these values to the Stern-Volmer equation enables the diffusional and environmental influences experienced by the dye to be described and ensures collisional quenching is involved.

3.3 *Cellular Application of Ruthenium(II)*

3.3.1 *Phototoxic effects on cell viability*

Coverslips, no. 1.5, ∅22 mm, within each chamber were marked with permanent marker pen to aid re-location of the specific cells exposed to laser excitation. Chambers were individually mounted into the heating plate on the inverted microscope stage and maintained at 37 °C within an environmental chamber set to 35 °C. The perpendicular lines were located using the eye piece and orientated so that the intersection was positioned in the top left corner of the field of view.

A single brightfield image was taken using the transmitted PMT and ×20 objective lens with a 2048×2048 format, two line averages and two frame average. Excitation was provided at 633 nm, via a helium-neon laser, to avoid direct excitation of $[Ru(bipy)_3]^{2+}$. This image was used to relocate the specific cells and FOV 24 h after excitation of $[Ru(bipy)_3]^{2+}$. A ×63 objective lens (NA = 1.4) was used with an image format, speed and laser repetition rate of 1024×1024, 400 Hz and MP 4 MHz, respectively, to select two cells for illumination per field of view. The image format was adjusted to 256×256 and a zoom in of the selected cell produced an image voxel size of 130×130 nm, half the Rayleigh criteria for maximum resolution, which will maximize possible photodamage. The selected cell was located centrally for maximum exposure and the detector switched to TCSPC PMT. The laser repetition rate was dropped to 500 kHz and EOM gain adjusted to provide a count rate $<5 \times 10^3$ counts/sec. The TCSPC parameters were also set to 256×256 image format and 256 time channels with a collection time of 1800 s.

After the laser exposure, agarose constructs were washed three times in media and continued incubation with 1 ml DMEM + 16%FBS for a further 24 h at 37 °C. Two cells were imaged per chamber and the procedure was repeated for a total of 11 cells. The control cells were treated in an identical manner and mounted on the microscope for the same length of time with the $[Ru(bipy)_3]^{2+}$, but without excitation.

Cellular viability was determined 24 h after excitation of $[Ru(bipy)_3]^{2+}$ including the corresponding control studies. The chambers were removed from the incubator, 5 μl/ml of Calcein AM and Ethdium homodimer-2 were added, and incubation continued for an additional 1 h. Brightfield images from the previous day were used to locate each exposed cell by realigning the perpendicular lines in the FOV. The FITC and TRITC programs were run on the Leica using an argon laser calibrated to an ex 488 nm and an em 500 to 535 nm and a He-Neon laser calibrated to/ex 543 nm and an em 555 to 700 nm, respectively. The pre-adjusted programs were placed into a sequence file and the selected cells imaged using two line and frame averages per image.

3.3.2 *Pericellular spatial oxygen gradient*

Chambers seeded at 4×10^6 cells/ml were mounted onto the stage of the inverted mircscope and maintained at 37 °C. Using the pulse-picked 4 MHz MP laser and an image format

of 512×512, an individual cell was identified and centrally located in the z-axis at ex 780 nm, and em 600 ± 50 nm. The repetition rate was then adjusted to 500 kHz, image format readjusted to 64×33, voxel size changed to 350×350 nm and field of view positioned to the right of the cell. In the Single Photon Counting Module, the ADC was set to 1024, image format was matched to the Leica and set to 64×33, photon collection rate was maintained at <1% of the repetition rate which is <5000 counts/s and the collection time was set to 900 s for each image. This procedure was repeated for each of the 52 cells. Control experiments were performed on agarose constructs prepared in an identical manner, but without cells.

Lifetime images were processed in Time Resolved Imaging software TRI2, Version 2.3.9.1.[42] Analysis of preliminary lifetime maps showed considerable high frequency spatial heterogeneity. Normal processing methods allow for binning to occur at increasing square sizes to increase pixel counts, however, they bare no relation to the subject of interest. Alternatively, TRI2 allows a masking feature where any pattern can be designed. Therefore, in order to determine the existence of any spatial oxygen gradients, as might be produced by cellular oxygen consumption, a circumferential binning mask was created and moved radially in incremental steps of one pixel creating a set of 59 masks. This method loses circumferential spatial information, but retains high spatial resolution in the radial x-axis.

Each drawn mask was loaded individually on to each FLIM intensity image where the counts in the mask were transferred for time resolved analysis and binned to produce a lifetime decay, as shown in Figs. 3(a) through 3(d). Individual pixels,

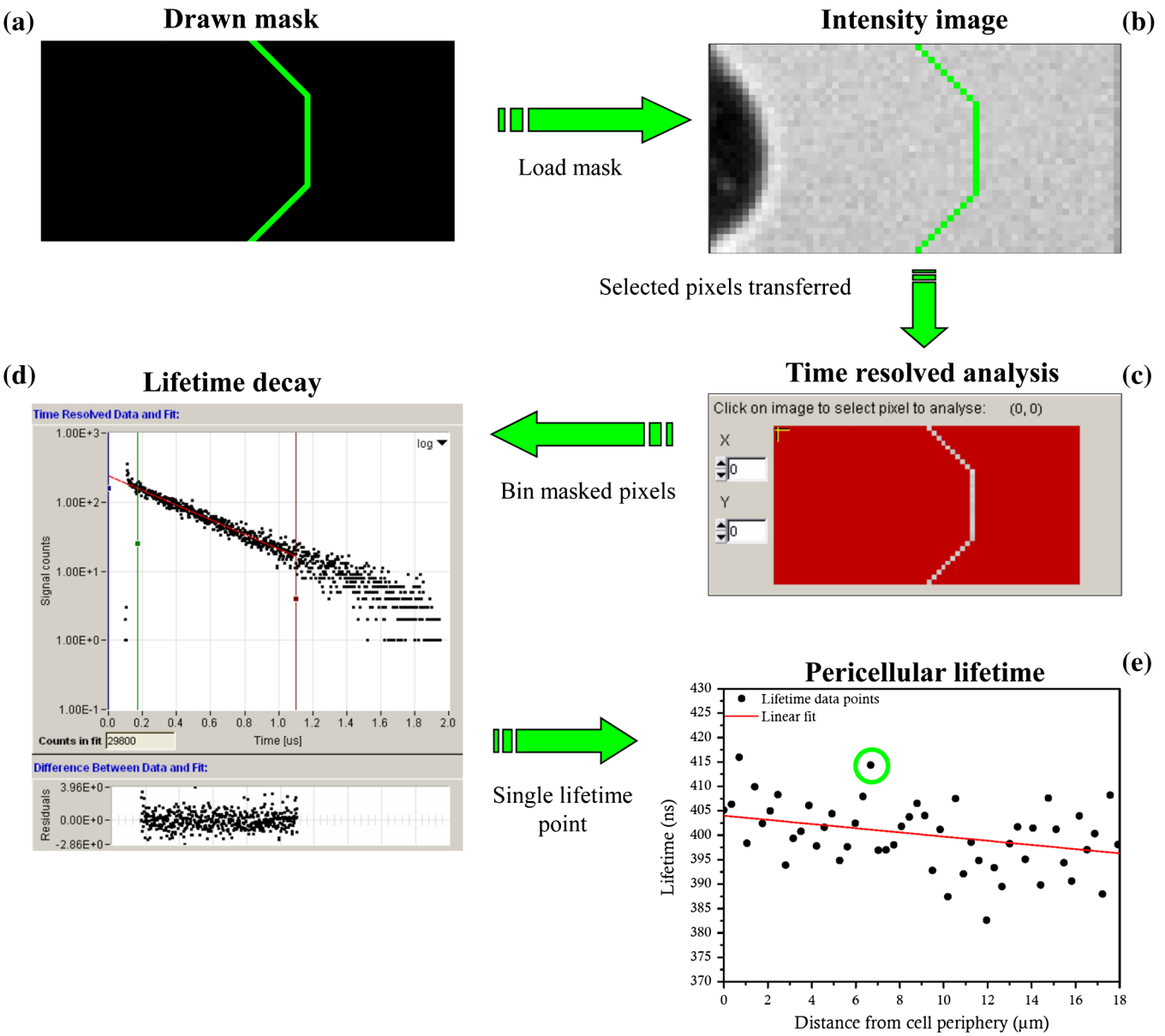

Fig. 3 Diagrammatic representation of the lifetime data analysis process. (a) A user user defined mask is illustrated in green; (b) the mask is applied to an intensity image of an unresolved test cell; (c) only the selected pixels in the mask are transferred for time resolved analysis; (d) pixels are binned to produce a single lifetime decay and mono-exponential fit applied with weighted residual below and (e) calculated lifetime is transferred to graph and positioned at mask distance represented by green circle. Other separate masks are created along the entire image to produce a complete data set of lifetime values versus distance from the cell periphery.

without binning, had accumulated between 450 and 800 counts/pixel and after masked binning contained between 16,000 and 25000 counts/decay. Each decay was individually analyzed using a mono-exponential model following a Levenberg-Marquardt fitting to determine τ where, Z is the offset, A is the amplitude and t is the time, as shown in Eq. (2).

$$f(t) = Z + A\exp^{(-t/\tau)}. \quad (2)$$

Repeated iterations of Chi-square, χ_r^2, were performed until $\chi_r^2 < 1.25$ with an offset fixed to zero. The derived lifetime of each mask represented single points at discrete distances from the cell as shown in Fig. 3(e). The lifetime values of each mask and cell were extracted from excel files, using Matlab, and imported into Origin. The mask lifetimes of each cell were plotted against distance from the cell edge and data points analyzed. Confirming whether a significant change of lifetime was seen with distance, a linear fit was applied at close proximity to the cell, although this would not be assumed for cellular consumption over larger distances. Conversion into oxygen concentration was performed as described by Gnaiger et al.[43] and units follow the recommended standard stated in the International Units of Physics and Chemistry (IUPAC) of mol/kg for gas concentrations in liquid.

4 Results

4.1 *Ruthenium Characterization*

4.1.1 $[Ru(Bipy)_3]^{2+}$ *Shows temperature dependence*

Figure 4 shows the influence of temperature on the lifetime response of $[Ru(bipy)_3]^{2+}$. Representative semi-log lifetime plot, represented in Fig. 4(a), show a reduction in gradient and lifetime with increasing temperature. The standard deviation for the fitting of each lifetime is <0.2%. The mean lifetime values from Fig. 4(a) at each temperature are plotted in Fig. 4(b) and demonstrate a statistically significant linear correlation over this temperature range. The error bars represent the standard deviation in lifetime and temperature from the five repeated measurements. The data lies within the upper and lower confidence limits of the relationship reported by Morris.[44]

4.1.2 *No correlation between* $[Ru(bipy)_3]^{+2}$ *lifetime and pH*

The stock solution of $[Ru(bipy)_3]^{2+}$ was dissolved in phosphate buffer between pH 5 and 7.5 to produce a final $[Ru(bipy)_3]^{2+}$ concentration of 0.412 mM. Repeated lifetime measurements at room temperature were taken of each pH concentration. There was no correlation between lifetime and pH concentration between 5 and 7.5 pH. The mean and standard deviation of the measured lifetimes were calculated as 388.4 ± 0.76 ns ($\pm 0.19\%$), respectively.

4.1.3 *Fetal bovine serum (FBS) shields* $[Ru(bipy)_3]^{2+}$ *from quenching*

The emission wavelength of increasing concentration of FBS diluted in deionised water with $[Ru(bipy)_3]^{2+}$ are presented in Fig. 5(a). All emission spectra show identical profiles regardless of percentage FBS concentration with asymmetric

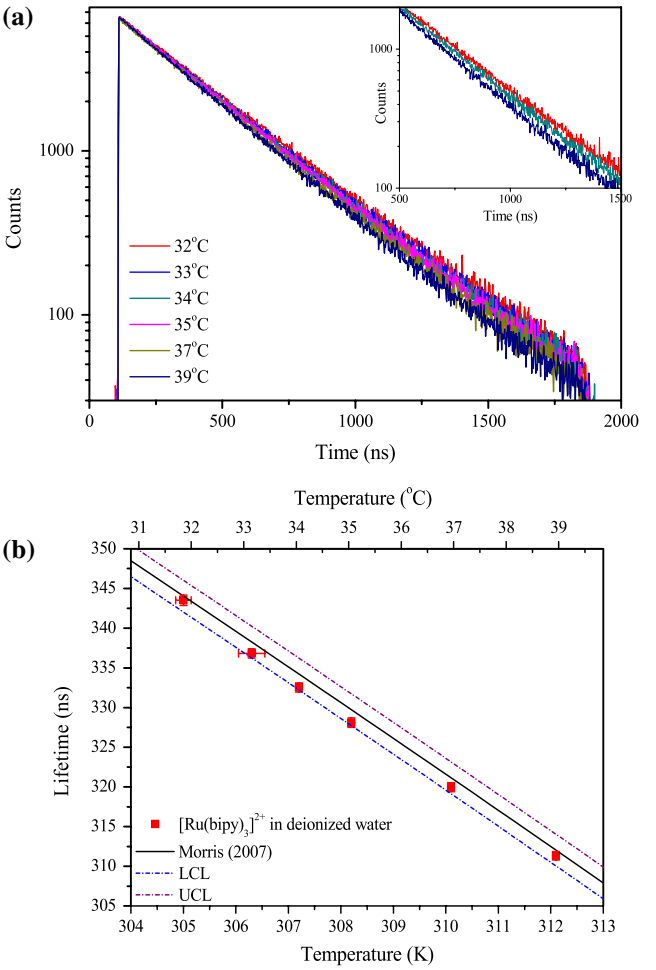

Fig. 4 Response of $[Ru(bipy)_3]^{2+}$ in deionzied water to a change in temperature. (a) Semi-log plot showing decay of photon counts with time and the effect induced by temperature. Inset: the central section of the decay between 500 to 1500 s displaying the shift in gradient when $[Ru(bipy)_3]^{+2}$ is exposed to 32 °C is represented by a red line, 34 °C is represented by a green line, and 39 °C is represented by a dark blue line. (b) The corresponding relationship between lifetime and temperature is shown as the lifetime measurements which are represented by red squares with error bars in x-axis representing temperature drift and error bars y-axis representing standard deviation of fit. Measured data is compared with Morris[44] which is indicated by a black line shown with upper and lower confidence (>95%) limits which are indicated by a purple dot dash line and a blue dot dash line, respectively.

responses. An asymmetric double sigmoidal peak function was used to determine the peak emission and FWHM as 608.1 ± 0.64 ns and 60.1 ± 0.64 ns, respectively.

The mean lifetime and intensity of the samples in Fig. 5(a) were plotted against increasing percentage of FBS in solution at ambient temperatures, as shown in Fig. 5(b). The standard deviations for the data of both lifetime and intensity were between 1% and 0.29% of the measurement at a given FBS concentration. Measurements for lifetime and intensity were acquired using the same sample. Both display an identical response to the increase in FBS concentration with an initial change in lifetime at increasing concentration that, subsequently, plateaus at the higher concentrations. Both sets of data have been fitted with a dose response curve, with adjusted $R^2 > 0.96$, reaching a maximum for the lifetime and intensity at 389.1 ns and 56702,

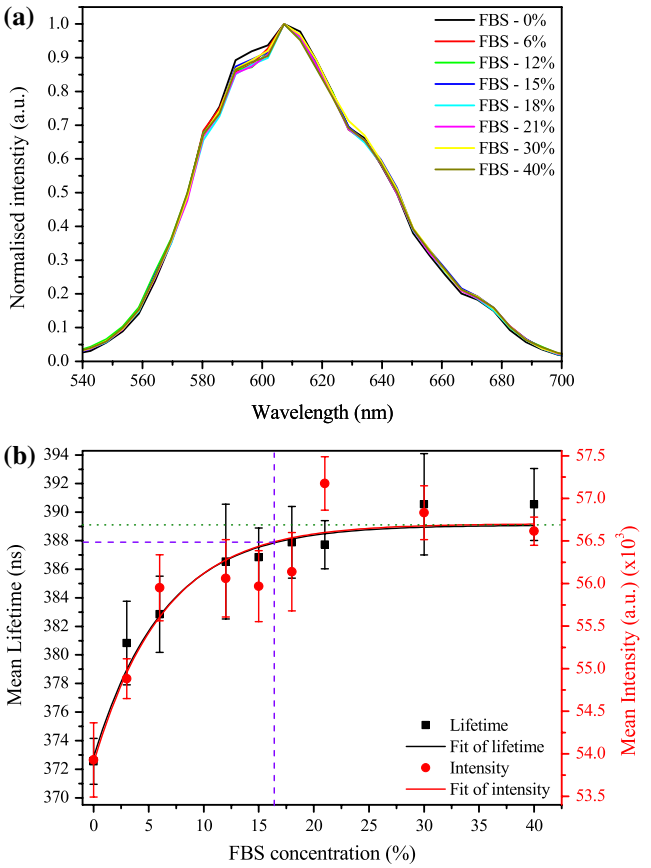

Fig. 5 Response of $[Ru(bipy)_3]^{2+}$ to concentrations of FBS diluted in de-ionized water. (a) Normalised intensity emission wavelength at an excitation of 780 nm and repetition rate of 500 kHz across an emission range of 540 to 700 nm. (b) Mean intensity and lifetime decays of $[Ru(bipy)_3]^{2+}$ with increment concentrations of FBS. Error bars represent standard deviations. Left and right *y*-axes correspond to the lifetime and intensity which are represented by black squares and red circles, respectively. Data points are fitted with a dose response curve using an adjusted $R^2 > 0.96$. The percentage of FBS in the cell culture media is represented by the purple dashed line which corresponds to a lifetime of 388 ns. The maximum response is represented by the dotted green line with a lifetime of 389 ns and intensity of 56702.

respectively, represented by the green dotted line. The percentage of FBS used in the cell culture media was 16%, represented by the purple dashed line, reaches a point on the curve that corresponds to a lifetime of 387.9 ns. The difference between the lifetime at the cell culture concentration and the maximum response of the fitted lifetime was 0.28%.

4.1.4 *Oxygen has linear relationship with* $[Ru(bipy)_3]^{+2}$

Lifetime measurements of $[Ru(bipy)_3]^{2+}$ dissolved in water and media at a temperature of 37 °C have been acquired at incrementing concentrations of dissolved oxygen, as shown in Fig. 6(a). A linear correlation can be seen between lifetime and oxygen molality this is characterized by the following negative linear models with an adjusted $R^2 > 0.98$:

$$\tau_{\text{water}} = 464.9 \times 10^{-9} \quad 689.1 \times 10^{-6} \cdot [O_2] \ (\text{mol/kg}); \quad (3)$$

$$\tau_{\text{media}} = 460.4 \times 10^{-9} \quad 616.9 \times 10^{-6} \cdot [O_2] \ (\text{mol/kg}). \quad (4)$$

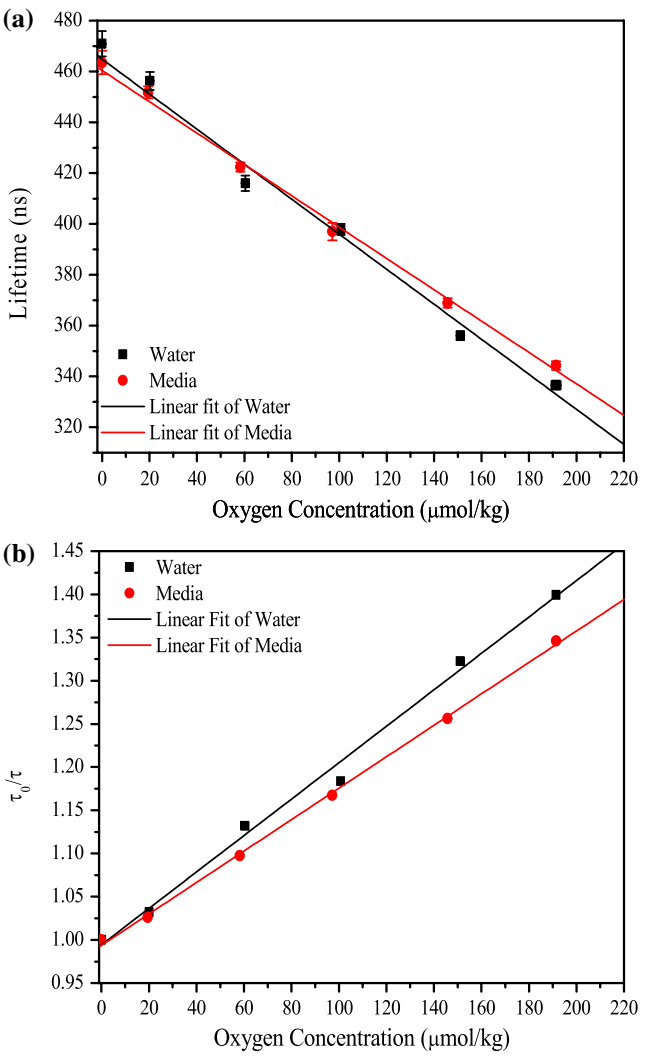

Fig. 6 Establishing a relationship lifetime and oxygen $[Ru(bipy)_3]^{2+}$ in solutions of de-ionized water, indicated by black squares and culture media, indicated by red circles, at 37 °C. (a) The mean lifetime values for water and culture are fitted with linear models. Vertical error bars represent an oxygen concentration accuracy of ±0.1% of the Xvivo system and horizontal error bars the standard deviation for the sample of lifetime measurements at each oxygen concentration. (b) The relationship between oxygen concentration and τ_0/τ was fitted by linear models to determine k_{sv} water and media as indicated by black squares and red circles, respectively.

The measured τ_0 for de-ionized water and media was 470.9 ns and 463.5 ns, respectively. By rearranging Eqs. (3) and (4), the oxygen molality can be calculated from the measured lifetime by applying Eq. (1), which produces Fig. 6(b).

Figure 6(b) depicts the ratio of τ_0/τ plotted against oxygen molality for $[Ru(bipy)_3]^{2+}$ in water and in media. Linear fits of both sets of data show a positive linear relationship between the ratio τ_0/τ and oxygen molality. The gradient for water is steeper than for media, but both intercept at approximately 1. The determined Stern-Volmer constant can now be used to calculate the bimolecular rate for $[Ru(bipy)_3]$ in water and media at 37 °C using Eq. (1) $k_{sv_{\text{water}}} = 2108.8$ mol/kg, $k_{sv_{\text{media}}} = 1819.8$ mol/kg, $k_{2,\text{water}} = 4.478 \times 10^9$ mol/kg/s, $k_{2,\text{media}} = 3.926 \times 10^9$ mol/kg/s, respectively.

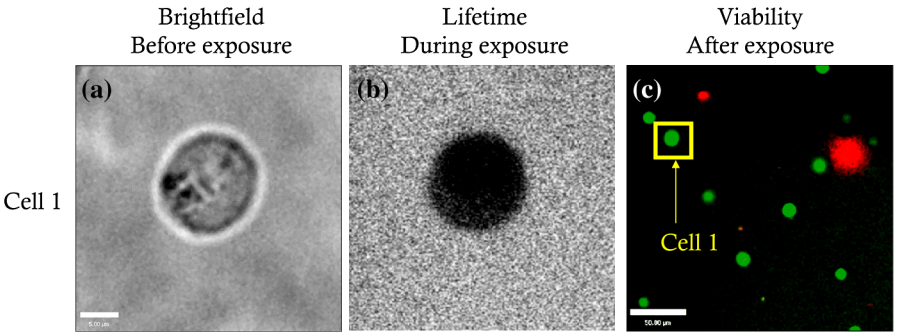

Fig. 7 Process of selecting and identification of cell 1 prior to after exposure to assess viability. (a) Brightfield image of identified cells before exposure, scale bar = 50 μm. (b) Lifetime image cells exposed to the imaging protocol and then chamber returned to the culture incubator for 24 h. (c) Same cells relocated using Brightfield and imaged using 488 nm and 564 nm excitation to reveal cells labelled with calcien AM and EthD-2. Live cells are illustrated in green, whereas, dead cells are illustrated in red with a scale bar = 50 μm.

4.2 *Interaction of $[Ru(bipy)_3]^{2+}$ with Cells*

4.2.1 *Phototoxicity of $[Ru(bipy)_3]^{2+}$*

Using the transmitted images, it was possible to relocate and identify the same cell 24 h after excitation of $[Ru(bipy)_3]^{2+}$ and to assess viability, as illustrated in Figs. 7(a)–7(c). The percentage viability 24 h after exposure was 90% with an identical 90% viability for control cells.

4.2.2 *A spatial oxygen gradient exists around a sub-population of chondrocytes*

The lifetime values acquired from each mask were converted to oxygen concentrations using a rearranged form of Eq. (1) and derived values from section 4.1.4 correlated with the central voxel distance from the cell periphery. In Figs. 8(a) and 8(b), two cells are displayed with oxygen concentration at an incrementing distance from the cell periphery, represented as zero μm. Figure 8(a) represents a cell displaying no statistically significant gradient or slope originating at the cell periphery, whereas, Fig. 8(b) displays a statistically significant positive gradient or slope that has developed from the cell periphery, reflecting a lower oxygen concentration close to the cell which would be compatible and expected with cellular consumption.

Performing this conversion for all the measured cells revealed a sub-population of 54% of cells in agarose gel, had no statistically significant correlation between oxygen concentration and distance from the cell periphery, as shown in Fig. 8(c). For the other 46% of cells, there was a statistically significant positive correlation. Only 4 percent of cells (52) showed a negative gradient, however, neither of these were statistically significant and matched that seen for agarose with no cells. The average gradient for the significant, non-significant and no cells was 0.53 ($\pm$0.11), 0.21 ($\pm$0.16) and 0.02 ($\pm$0.11) μmol/kg/μm, respectively. The cells associated with statistically significant oxygen gradients were larger than those with no statistical significant gradient with median values of 12.5 and 10.9 μm, respectively. This difference in cell size was statistically significant based upon a Mann-Whitney U-test ($p < 0.05$).

5 Discussion

The development of a pulse-picked TP confocal system required the characterisation of $[Ru(bipy)_3]^{2+}$ within its intended environment in order to understand the restrictions, limitations and the sensitivity to its application for pericellular spatial oxygen quantification. This involved investigating possible effect from temperature, pH, cell culture media and characterizing the relationship between lifetime and oxygen concentration.

There was a negative correlation between temperature and lifetime measurements, in accordance with findings by other researchers.[44–46] In Fig. 4 the relationship between lifetime and temperature appears to be linear. However, over a larger temperature range, previous studies have shown that the relationship is best represented by a polynomial.[44] An increase in the temperature of water reduces dissolved oxygen and, therefore, should reduce quenching and increase the lifetime. At the same time, there is an increase in the rate of diffusion and therefore collisional quenching. Studies of the temperature effect on $[Ru(bipy)_3]^{2+}$ without oxygen present have shown that this relationship is due to the thermal activation of a non-radative pathway that operates via the non-luminescent d-d energy state.[44–46] For example, a change of 1 °C in $[Ru(bipy)_3]^{2+}$ in aqueous solution can induce a 1% change in the lifetime. This highlights the vital importance of maintaining stable and reliable temperature control system to obtain accurate results when using $[Ru(bipy)_3]^{2+}$.

Altering pH to mimic the physiological range, 5 to 7.5 pH, did not affect the measured $[Ru(bipy)_3]^{2+}$ lifetime. This finding was consistent with previous studies.[33] The variability between the measurements across all pH levels shows a standard deviation of <0.19%.

The emission spectra showed identical profiles and no spectral shift for increasing concentrations of FBS in water + $[Ru(bipy)_3]^{2+}$. No spectral shift suggests that there is no physical binding to ruthenium(II) and that only one population of fluorophores are emitting.[21]

Examining the lifetime and intensity measurements of $[Ru(bipy)]^{2+}$, with increasing concentrations of FBS, reveals similar responses with a positive correlation that gradually decreases to disassociation as illustrated in Fig. 5(b). Since both the lifetime and intensity increase, this indicates that there is less oxygen quenching the fluorophore. However, as the overall oxygen concentration has not been changed, it suggests that the FBS must be abating the oxygen surrounding the $[Ru(bipy)_3]^{2+}$. This is supported by previous studies by Vaughan and Weber, [22] who looked at pyrenebutyric acid as a dynamic probe for microenvironments. They showed that if pyrenebutyric acid was conjugated to bovine serum albumin,

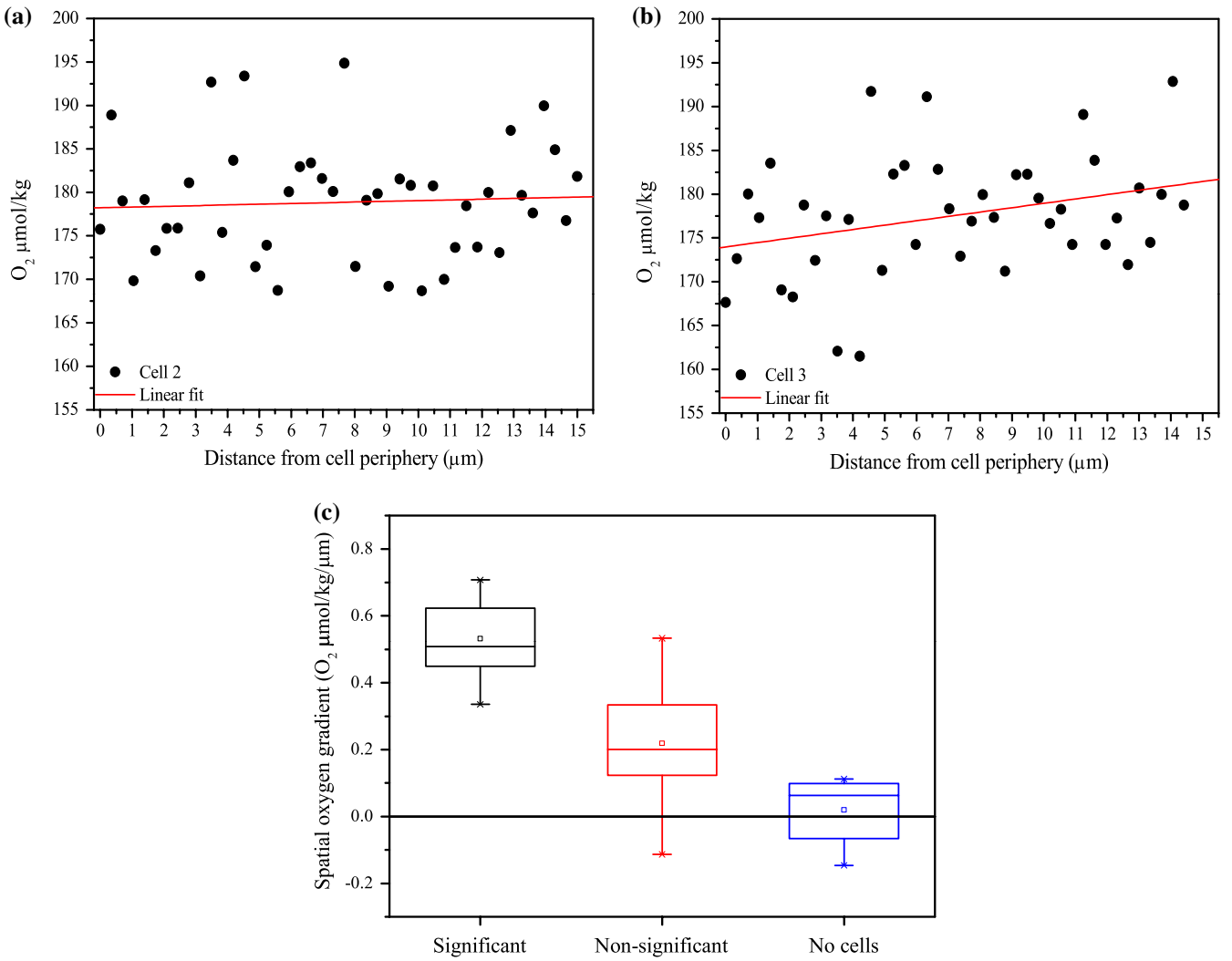

Fig. 8 Converted lifetime data of representative cells showing spatial variation in oxygen concentration with distance from the periphery and the oxygen spatial gradients of cells in a population. All cells have been fitted with linear models assumed at close proximity to the cell to provide the spatial oxygen gradient. (a) For cell 2, the linear model shows no statistically significant correlation. (b) For cell 3, there is a significant positive correlation with a gradient of 0.5 μmol/kg/μm and pericellular oxygen concentration of 174 μmol/kg. (c) Box and whiskers plot of spatial oxygen gradients derived from assumed linear models at close proximity to the cell which have been fitted to data sets of change in oxygen concentration versus distance from the cell periphery. Whiskers and box represent outliers and 25&75 quartiles respectively.

there was no response to changes in oxygen. However, when free in solution, there was a positive linear relationship. Lakowicz and Weber[47] stated that this effect is caused by the protein structure that prevents the diffusion of oxygen reaching the fluorophore. However, the fluorophores used in these previous studies were conjugated to bovine serum albumin and showed a slightly different response between the intensity and lifetime measurements. This was a combination of static and dynamic quenching, where the intensity measurements were unaffected by bovine serum albumin concentration and produced a linear response. The lifetime measurements only produced a partial response and then became static, as found in the current study.[47] This suggests that $[Ru(bipy)_3]^{2+}$ is not conjugated to FBS or its constituents. This was further supported by the fact that there was no shift in the emission spectra. Similar effects are also seen when $[Ru(bipy)_3]^{2+}$ comes into contact with DNA. In this case, it can become electrostatically bound or can exhibit partial intercalation depending on the ratio of dye and DNA.[48] It has been shown by Jain et al.[32] that $[Ru(bipy)_3]^{2+}$ has the weakest binding of all ruthenium(II) complexes to DNA, proteins and serum, due to the presence of hydrophobic organic ligands. This suggests that FBS is partially shielding $[Ru(bipy)_3]^{2+}$ from oxygen until the FBS increase in concentration has shielded all $[Ru(bipy)_3]^{2+}$. At this point, no further response is seen with increasing FBS concentrations. In theory, it would then be expected to change with increasing concentrations of the dye.

Experiments have confirmed that there is a negative linear relationship between lifetime and oxygen molality. As the oxygen partial pressure increases, so does the molality leading to fluorescence quenching and a decrease in lifetime. The τ_0 for water and culture media containing FBS are different, which indicates that some form of electrostatic binding could be affecting the radiative rates, as was observed for the interaction between water and FBS in section 4.1.3. The linear fits that establish the relationship between $[Ru(bipy)_3]^{2+}$ in water and media display smaller standard deviations for media than for water, as illustrated in Fig. 6(a). This indicates that the dye is

less sensitive to the environmental change, such as oxygen concentration or temperature fluctuations, when in media. The Stern-Volmer plots indicate dynamic quenching is involved due to the linear lifetime measurement.[21] This relationship has also been confirmed by other researchers.[49,50] The difference in the Stern-Volmer gradients between water and media reflects different bimolecular quenching interactions. The K_{SV} values are reflective of the fluorophores environment, such as the influence of temperature, viscosity and binding. A large effect to K_{SV} was reported by Maheswari et al. [51], where $[Ru(bipy)_3]^{2+}$ was measured in the presence of DNA due to electrostatic intercalation with DNA base pairs. The effect of binding is apparent in Maheswari et al. [51] data with an 83% greater K_{SV} value in comparison to the current study for $[Ru(bipy)_3]^{2+}$ in media. This confirms that $[Ru(bipy)_3]^{2+}$ in media is not bound, but rather has a restrictive quenching relationship. Instead of using the Smoluchowki's equation to calculate k_0, Demas et al. [41] and Rusak et al.[50] used Debye's approximate equation[52] which assumed that the size and the specific molecules were unimportant, and only the temperature and viscosity of the solvent need to be considered. Equation 5 shows their applied equation[50]:

$$k_0 = \frac{8RT}{3\eta}, \tag{5}$$

where, T is the temperature (K), R is the gas constant (8.314472×10^2 L.Pa/mol.K) and η is the viscosity (kg/m/l). Using this same equation and applying it to the values of the current studies, it provides $k_0 = 9.968 \times 10^9$ M/s. Applying k_0 to the frequency of collisions, calculates 0.449 and 0.394 for water and media, respectively. The frequency of collision for water is identical with the value derived by Rusak et al.,[50] however the media value is 14% less than in water.

Cells maintained >90% viability after 1800 s of laser exposure to the surrounding $[Ru(bipy)_3]^{2+}$, at a concentration of 0.412 mM. This is in contradiction to the phototoxicity reported by Dobrucki, when macrophages were exposed to confocal imaging in the presence of $[Ru(bipy)_3]^{2+}$ at concentrations of 0.2 mM, and with 112 illuminations.[33] However, other researchers have used concentrations up to 1.34 mM with no reported loss of viability.[49] The difference stems from the power of the excitation, which governs the generation of reactive oxygen species created by oxygen quenching $[Ru(bipy)_3]^{2+}$, and confirms the variability in phototoxicity between different imaging protocols and excitation methods. Dobrucki states, that the high pressure mercury arc lamp used in their experiments delivered a light beam with 0.1 mW of light focused onto a diffraction limited spot delivering 0.16 J/cm^2 for one scan/pixel. The current systems excitation wavelength was 780 nm at 500 kHz repetition rate and had a 160 μW of average power at the sample. The energy per pulse E, is calculated as 3.2×10^{-10} J using Eq. (6):

$$E = \frac{P}{R_r}, \tag{6}$$

where, P is the power and R_r is the repetition rate. The fluency can then be calculated by dividing the energy by the area of the beam exposure. The pixel size was 130×130 nm, so assuming a circular beam diameter of 130 nm, the fluency can be calculated as 2.46 J/cm^2. This fluency is 15 times higher than the value calculated by Dobrucki, and suggests that the slow repetition rate provides the damaging free radicals time to diffuse away from the illuminated area. These experiments confirm that the current imaging protocol and $[Ru(bipy)_3]^{2+}$ concentration are suitable for the assessment of lifetime, without affecting chondrocyte viability in agarose.

Analyzing the relationship between oxygen concentration and distance from the cell periphery has shown that 98% of cells show a positive oxygen gradient such that oxygen concentration reduces close to the cell. There was some variability in the magnitude of this gradient with a sub-population of 46% of cells for which correlation between oxygen and distance was statistically significant, as well as, having a statistically larger cell diameter. None of the gradients measured from the population displayed any statistically significant negative spatial oxygen gradients. This is consistent with the fact that all cells are consuming oxygen, although some do so at a faster rate. This variability in apparent oxygen consumption may reflect the known heterogeneity of the chondrocyte population,[53,54] with larger, more metabolically active cells from the deep zone of articular cartilage being those cells with a greater statistically significant oxygen gradient.

6 Conclusion

A TCSPC based TP confocal, with added pulse-picker, was used for the detection of $[Ru(bipy)_3]^{2+}$ lifetime response to changes in oxygen concentration. This was specifically applied to extract high spatial resolution at close proximity to the cell periphery. It was established that $[Ru(bipy)_3]^{2+}$ was independent of pH concentration, however, it was susceptible to variations in serum concentration and temperature. We suggest that $[Ru(bipy)_3]^{2+}$ temperature dependence can be linearly described over short temperature ranges, 32 to 39 °C, and that the addition of FBS creates a shielding effect from oxygen quenching forming a concentration dependence and slightly reducing $[Ru(bipy)_3]^{2+}$ sensitivity to fluctuations in its environment.

The optimized protocol maintained chondrocyte viability at >90% and was effective in quantifying pericellular spatial oxygen gradients with a high degree of accuracy and reproducibility. This demonstrated that living cells *in-vitro* establish a self-induced pericellular oxygen gradient, which was successfully quantified using the implemented TCSPC FLIM system. The extrapolation of this technique to *in-vivo* studies is complex due to environmental effects, such as protein binding, which cannot be so easily controlled. However, the present study provides a powerful technique for *in-vitro* investigation of cellular oxygen consumption and its associated spatial gradients. Such experimental studies will support further *in silico* modeling approaches for understanding oxygen consumption and microenvironment both *in-vitro* and *in-vivo*.

Acknowledgements

This work was supported by Biotechnology and Biological Sciences Research Council which was part of a Collaborative Awards in Science and Engineering studentship and was also supported via an Engineering and Physical Sciences Research

Council platform grant. We would like to acknowledge Klaus Suhling in the helpful discussions that contributed to this work.

References

1. S. Zhou, Z. Cui, and J. P. G. Urban, "Factors influencing the oxygen concentration gradient from the synovial surface of articular cartilage to the cartilage-bone interface: a modeling study," *Arthritis Rheum.* **50**(12), 3915–3924 (2004).
2. L. Zhang and J. Siepmann, "Direct calculation of Henry's law constants from Gibbs ensemble Monte Carlo simulations: nitrogen, oxygen, carbon dioxide and methane in ethanol," *Theor. Chem. Accounts Theor Comput. Model. Theor. Chim. Acta* **115**(5), 391–397 (2006).
3. M. C. Krishna et al., "Overhauser enhanced magnetic resonance imaging for tumor oximetry: coregistration of tumor anatomy and tissue oxygen concentration," *Proc. Natl. Acad. Sci. U.S.A.* **99**(4), 2216–2221 (2002).
4. S. Matsumoto et al., "Low-field paramagnetic resonance imaging of tumor oxygenation and glycolytic activity in mice," *J. Clin. Invest.* **118**(5), 1965–1973 (2008).
5. W. Wang and P. Vadgama, "O2 microsensors for minimally invasive tissue monitoring," *J. R. Soc. Interface* **1**(1), 109–117 (2004).
6. M. J. Grimshaw and R. M. Mason, "Bovine articular chondrocyte function in vitro depends upon oxygen tension," *Osteoarthr. Cartil.* **8**(5), 386–392 (2000).
7. M. C. Lewis et al., "Heterogeneous proliferation within engineered cartilaginous tissue: the role of oxygen tension," *Biotechnol. Bioeng.* **91**(5), 607–615 (2005).
8. K. Mamchaoui and G. Saumon, "A method for measuring the oxygen consumption of intact cell monolayers," *Am. J. Physiol. Lung Cell Mol. Physiol.* **278**(4), L858–863 (2000).
9. W. Y. Gu et al., "Diffusivity of ions in agarose gels and intervertebral disc: effect of porosity," *Ann. Biomed. Eng.* **32**(12), 1710–1717 (2004).
10. U. Cheema et al., "Spatially defined oxygen gradients and vascular endothelial growth factor expression in an engineered 3D cell model," *Cell. Mol. Life Sci.* **65**(1), 177–186 (2008).
11. Unsense, "Oxygen sensors," http://www.unisense.com (2010).
12. F. G. Gao, A. S. Jeevarajan, and M. M. Anderson, "Long-term continuous monitoring of dissolved oxygen in cell culture medium for perfused bioreactors using optical oxygen sensors," *Biotechnol. Bioeng.* **86**(4), 425–433 (2004).
13. G. Mehta et al., "Quantitative measurement and control of oxygen levels in microfluidic poly(dimethylsiloxane) bioreactors during cell culture," *Biomed. Microdev.* (2006).
14. S. B. Bambot, G. Rao, M. Romauld, G. M. Carter, J. Sipior, E. Terpetchnig, and J. R. Lakowicz, "Sensing oxygen through skin using a red diode laser and fluorescence lifetimes," *Biosens. Bioelectron.* **10**(6–7), 643–652 (1995).
15. D. Elson et al., "Time-domain fluorescence lifetime imaging applied to biological tissue," *Photochem. Photobiol. Sci.* **3**(8), 795–801 (2004).
16. E. Gratton et al., "Fluorescence lifetime imaging for the two-photon microscope: time-domain and frequency-domain methods," *J. Biomed. Opt.* **8**(3), 381–390 (2003).
17. J. Philip and K. Carlsson, "Theoretical investigation of the signal-to-noise ratio in fluorescence lifetime imaging," *J. Opt. Soc. Am. A* **20**(2), 368–379 (2003).
18. W. Becker et al., "Fluorescence lifetime images and correlation spectra obtained by multidimensional time-correlated single photon counting," *Microsc. Res. Tech.* **69**(3), 186–195 (2006).
19. J. Requejo-Isidro et al., "High-speed wide-field time-gated endoscopic fluorescence-lifetimeimaging," *Opt. Lett.* **29**(19), 2249–2251 (2004).
20. W. Becker et al., "Fluorescence lifetime imaging by time-correlated single-photon counting," *Microsc. Res. Tech.* **63**(1), 58–66 (2004).
21. J. R. Lakowicz and SpringerLink, *Principles of fluorescence spectroscopy*, Springer, New York (2006).
22. W. M. Vaughn and G. Weber, "Oxygen quenching of pyrenebutyric acid fluorescence in water. Dynamic probe of the microenvironment," *Biochemistry* **9**(3), 464–473 (1970).
23. J. Ji et al., "Novel fluorescent oxygen indicator for intracellular oxygen measurements," *J. Biomed. Opt.* **7**(3), 404–409 (2002).
24. R. L. Plant and D. H. Burns, "Quantitative, depth-resolved imaging of oxygen concentration by phosphorescence lifetime measurement," *Appl. Spectrosc.* **47**(10), 1594–1599 (1993).
25. T. Rharass et al., "Variation of 1-pyrenebutyric acid fluorescence lifetime in single living cells treated with molecules increasing or decreasing reactive oxygen species levels," *Anal. Biochem.* **357**(1), 1–8 (2006).
26. M. A. Yaseen et al., "Optical monitoring of oxygen tension in cortical microvessels with confocal microscopy," *Opt. Express* **17**(25), 22341–22350 (2009).
27. E. G. Mik van et al., "Quantitative determination of localized tissue oxygen concentration in vivo by two-photon excitation phosphorescence lifetime measurements," *J. Appl. Physiol.* **97**(5), 1962–1969 (2004).
28. H. C. Gerritsen et al., "Fluorescence lifetime imaging of oxygen in living cells," *J. Fluoresc.* **7**(1), 11–15 (1997).
29. T. Itoh et al., "In vivo visualization of oxygen transport in microvascular network," *Am. J. Physiol.* **267**(5), H2068–2078 (1994).
30. Y. Amao, "Fundamental review: probes and polymers for optical sensing of oxygen," *Microchim. Acta* **143**(1), 1–12 (2003).
31. E. R. Carraway et al., "Photophysics and photochemistry of oxygen sensors based on luminescent transition-metal complexes," *Anal. Chem.* **63**(4), 337–342 (1991).
32. A. Jain et al., "Binding of luminescent ruthenium(II) molecular probes to vesicles," *Inorg. Chem.* **37**(8), 1876–1879 (1998).
33. J. W. Dobrucki, "Interaction of oxygen-sensitive luminescent probes $[Ru(phen)_3]^{2+}$ and $[[Ru(bipy)_3]^{2+}$ with animal and plant cells in vitro: mechanism of phototoxicity and conditions for non-invasive oxygen measurements," *J. Photochem. Photobiol., B* **65**(2–3), 136–144 (2001).
34. Z. J. Fuller et al., "Photostability of luminescent ruthenium(II) complexes in polymers and in solution," *Anal. Chem.* **75**(11), 2670–2677 (2003).
35. N. A. Hosny, D. A. Lee, and M. M. Knight, *Proc. SPIE* **7569**, 756932 (2010)
36. W. Becker, *Advanced Time-Correlated Single Photon Counting Techniques*, Springer, Berlin, New York (2005).
37. D. V. O'Connor and D. Phillips, *Time-Correlated Single Photon Counting*, Academic, London (1984).
38. T. T. Chowdhury, D. L. Bader, and D. A. Lee, "Dynamic compression counteracts IL-1[beta]-induced release of nitric oxide and PGE2 by superficial zone chondrocytes cultured in agarose constructs," *Osteoarthr. Cartil.* **11**(9), 688–696 (2003).
39. M. Garcia and M. M. Knight, "Cyclic loading opens hemichannels to release ATP as part of a chondrocyte mechanotransduction pathway," *J. Orthop. Res.* **28**(4), 510–515 (2010).
40. H. K. Heywood et al., "Cellular utilization determines viability and matrix distribution profiles in chondrocyte-seeded alginate constructs," *Tissue Eng.* **10**(9–10), 1467–1479 (2004).
41. J. N. Demas, *Excited State Lifetime Measurements*, Academic Press, New York (1983).
42. P. R. Barber et al., "Multiphoton time-domain fluorescence lifetime imaging microscopy: practical application to protein-protein interactions using global analysis," *J. R. Soc. Interface* **6**(Suppl 1), S93–S105 (2009).
43. E. Gnaiger and H. Forstner, *Polarographic Oxygen Sensors: Aquatic and Physiological Applications*, Springer-Verlag, Berlin; New York (1983).
44. K. J. Morris et al., "Luminescence lifetime standards for the nanosecond to microsecond range and oxygen quenching of ruthenium(II) complexes," *Anal. Chem.* **79**(24), 9310–9314 (2007).
45. A. Juris et al., "Ru(II) polypyridine complexes: photophysics, photochemistry, eletrochemistry, and chemiluminescence," *Coord. Chem. Rev.* **84**(March), 85–277 (1988).
46. J. Van Houten and R. J. Watts, "Temperature dependence of the photophysical and photochemical properties of the tris(2,2'-bipyridyl)ruthenium(II) ion in aqueous solution," *J Chem. Soc.* **98**(16), 4853–4858 (1976).
47. J. R. Lakowicz and G. Weber, "Quenching of fluorescence by oxygen. A probe for structural fluctuations in macromolecules," *Biochemistry* **12**(21), 4161–4170 (1973).
48. H. Görner, C. Stradowski, and D. Schulte-Frohlinde, "Photoreactions of tris(2,2′-bipyridyl)-ruthenium(II) with peroxydisulfate in deoxygenated

aqueous solution in the presence of nucleic acid components, polynucleotides, and DNA.," *Photochem. Photobiol.* **47**(1), 15–29 (1988).
49. D. Sud et al., "Measurement of intracellular oxygen levels using fluorescence lifetime imaging microscopy (FLIM)," *Proc. SPIE* **5859**, 585907 (2005).
50. D. A. Rusak et al., "Investigation of fluorescence lifetime quenching of $[[Ru(bpy)_3]^{2+}$ by oxygen using a pulsed light-emitting diode," *J. Chem. Educ.* **83**(12), 1857 (2006).
51. P. U. Maheswari, V. Rajendiran, M. Palaniandavar, R. Thomas, and G. U. Kulkarni, "Mixed ligand ruthenium(II) complexes of 5,6-dimethyl-1,10-phenanthroline: the role of ligand hydrophobicity on DNA binding of the complexes," *Inorg. Chim. Acta* **359**(14), 4601–4612 (2006).
52. C. E. Wayne and R. P. Wayne, *Photochemistry*, Oxford University Press, Oxford (1999).
53. H. K. Heywood, M. M. Knight, and D. A. Lee, "Both superficial and deep zone articular chondrocyte subpopulations exhibit the crabtree effect but have different basal oxygen consumption rates," *J. Cell. Physiol.* **223**(3), 630–639 (2010).
54. S. Zhou, Z. Cui, and J. P. G. Urban, "Nutrient gradients in engineered cartilage: metabolic kinetics measurement and mass transfer modeling," *Biotechnol. Bioeng.* **101**(2), 408–421 (2008).